Nuclear Instruments and Methods in Physics Research A277 (1989) 599–607
North-Holland, Amsterdam

CALCULATION OF THE PULSE-HEIGHT RESPONSE OF ORGANIC SCINTILLATORS FOR NEUTRON ENERGIES $28 < E_n < 492$ MeV

W.C. SAILOR, R.C. BYRD and Y. YARIV *

Los Alamos National Laboratory, Los Alamos, NM 87545, USA

Received 22 November 1988

An adaptation of the Monte Carlo code of Stanton has been used to calculate the pulse-height spectra for monoenergetic neutrons incident on organic scintillators at energies $28 < E_n < 492$ MeV. Pulse-height distributions calculated with the code are compared to recent experimental results to determine the relative importance of various reaction channels and multiple scattering. The code has also been modified so that the effect of photon losses through attenuation and reflection is modeled for the first time. Changes in the reaction kinematics are discussed which might improve the code's predictive capabilities at neutron energies over 70 MeV.

1. Introduction

In neutron time-of-flight measurements at medium energies ($50 < E_n < 800$ MeV), flight paths of 50–600 m are necessary in order to obtain energy resolutions required to study transitions to discrete nuclear states separated by less than 1 MeV. Organic scintillators with volumes up to a few hundred liters are then needed to maintain adequate counting rates, and segmentation into as many as 30 individual elements has been used to preserve good time resolution.

For single-element detectors, the Monte Carlo code of Cecil et al. [1] has been shown to give fairly reliable reproduction of measured detection efficiencies for neutrons over a wide range of energies. Unfortunately, the code is of limited use for multi-element detectors [2–6], where it is much more important to have the correct charged-particle energy distributions and such effects as crosstalk due to multiple scattering cannot be neglected. The effects of light transport should also be considered in order to maintain good performance with large-volume scintillators.

Our goal is to develop a computer code which will produce essentially the same efficiency as the Cecil et al. code in the energy range $1 < E_n < 300$ MeV, but which can also be used for multi-element applications at neutron energies up to 800 MeV. As a test of the code's capabilities, we have looked in depth at its predictions of pulse-height spectra for single-element detectors as compared to experimental measurements. We show which features of the spectra are determined by the various reaction channels, by multiple scattering, and by photon losses. From the results we have obtained information about the modifications that will be needed to extend the applicability of the code.

2. Model background

The Cecil et al. code is a version of the Stanton [8] code which was altered first by McNaughton et al. [9] and then by Cecil. The Stanton code is in turn a Monte Carlo version of Kurz's [10] analytical code. Several other authors [11–16] have also produced codes, but they mostly differ from Kurz's or Stanton's code only in detail. Among the features included in the Cecil et al. code are relativistic reaction kinematics and estimation of signal loss from protons and alpha particles which escape from the detector volume. The light-output curves are of the form used by Madey et al. [18]. The appropriate reference should be consulted for further information about other modeling details.

To test the accuracy of the code for the prediction of integral efficiencies, Cecil et al. compared their results to experiments [9,19–29] at various energies up to 300 MeV. The code has also been tested by other groups [30–36], mostly against integral measurements, and found to agree with the data to within 10%. The exceptions appear to fall into two classes. The clearest discrepancies occur [24–26] at higher neutron energies (over 60 MeV) and low biases (between 1 and 3 MeV_{ee}). In particular, Young et al.'s [24] data, which are about 15% above the calculations, were obtained with a large NE102 scintillator (30.5 cm in thickness and 12.7 cm in diameter) at energies $80 < E_n < 160$ MeV and a bias of 2 MeV_{ee}. In addition, changes in the shape of the

* Permanent address: Non-Destructive Testing Department, Soreq Nuclear Research Center, Yavne 70600, Israel.

pulse-height spectrum at energies above 50 MeV are poorly described. Our measured spectrum near 50 MeV is reasonably well reproduced, but that near 80 MeV and one measured by Sakai et al. [36] at $E_n = 60$ MeV for an NE213 scintillator are both in serious disagreement with the predicted response. As explained in section 3, the problems with spectral shapes and with efficiencies at low thresholds for higher energies may both be due to the difficulty of modeling ^{12}C breakup reactions above 50 MeV.

The second general class of discrepancies relates to liquid scintillators at energies over 60 MeV, where agreement was better than 10% only for those less than 3 cm deep [33–35]. Our own integral measurements [7] for large NE213 and BC501 liquid scintillators at 25–200 MeV are as much as 20% different from the code results. These difficulties may be associated with complications unique to liquid scintillators, including uncertainty in active volumes, reactions with container walls, density effects in ranges and light outputs, variations in hydrogen/carbon ratios, and the generally poorer light transport in liquid scintillators.

3. Analysis of pulse-height spectra using the existing code

The pulse-height measurements used throughout this section were measured at the Indiana University Cyclotron Facility (IUCF) in an experiment described in a companion paper [7]. All results selected for discussion here are for a large, cylindrical BC501 scintillator 30.5 cm in diameter and 20.3 cm in thickness. As discussed in ref. [7], the spectra were multiplied by a factor of 1.14 in order to bring the integrated efficiencies into agreement with the calculations and with other measurements. The observed pulse-height scale was also adjusted so that the maximum observed light output matches the calculated result.

In the general version of the Cecil et al. code obtained from Kent State University, there are (quite properly) minimal assumptions about the details of a particular experimental setup. For all calculations in this section the original code was modified to include a resolution function and hardware threshold characteristic of our experiment. For the resolution function, a convenient and general approximation has been suggested [37]:

$$\left(\frac{\Delta E}{E}\right)^2 = \left(\frac{\sigma_n^2}{E^2} + \frac{\sigma_s^2}{E} + \sigma_p^2\right), \tag{1}$$

where E is the light output in MeV_{ee}. The first term is a constant factor due to electronic noise; its effect is most important at the lowest pulse heights. Its value was determined in the experiment to be 0.9 MeV_{ee}, except for the 78.4 MeV spectrum, where a value of 0.1 MeV_{ee} was obtained. The σ_s term reflects photon-counting statistics; its size was estimated from typical scintillator parameters as

$$\sigma_s = \sqrt{\frac{1}{P\epsilon Q}}\,, \tag{2}$$

where P is the number of photons from a 1 MeV electron in BC501 (65% of anthracene, or 9800 photons); ϵ is the fraction of photons created which enter the photomultiplier tube (taken as 10%, independent of position); and Q is the photomultiplier quantum efficiency (taken as 20%). The third resolution term is largely due to position nonuniformity in light production and collection; these effects are approximately proportional to pulse height and become more important at the upper end of the spectrum. A typical value of σ_p for a large scintillator is about 10%. Instead of estimating this value by fitting the measured spectra, we have explicitly calculated the effects of photon transport as described in section 4. The third term is therefore omitted from the calculations in this section.

The method chosen for calculating the resolution and threshold effects in our experiment was first to perform a Gaussian smoothing of the total pulse height with the width of the statistical component. Next, all events with pulse heights below the hardware threshold of 3.7 MeV_{ee} (10 MeV_{ee} for $E_n = 78.4$ MeV) were set to zero. Lastly, another smoothing with the width due to electronic noise was folded in. The interaction between detector resolution and the discriminators and ADCs used in the electronics cannot be modeled exactly, so comparisons of measurements and calculations near the hardware threshold should be made cautiously.

3.1. Pulse-height spectrum by reaction channel

Much of this paper concerns the particular set of model reaction channels employed in the Cecil et al. code. The most difficult problem is the treatment of the reaction channels where carbon breaks up to emit charged fragments. The original paper by Kellogg [17] gave 65 separate cross sections for neutron-induced carbon breakup in a cloud-chamber experiment at 90 MeV, and each channel produces one or more charged particles which contribute in some way to the detector response. In the Cecil et al. code all interactions are distributed among the following set of model reaction channels:

(1) $n + p \rightarrow n + p$ (elastic);
(2) $n + {}^{12}C \rightarrow n + {}^{12}C$ (elastic);
(3) $n + {}^{12}C \rightarrow n + {}^{12}C + \gamma$;
(4) $n + {}^{12}C \rightarrow \alpha + {}^{9}Be$;
(5) $n + {}^{12}C \rightarrow n + 3\alpha$;
(6) $n + {}^{12}C \rightarrow p + {}^{12}B$.

This grouping of reactions is clearly a great simplification, and for this reason it cannot be expected to give accurate charged-particle energy distributions or pulse-height spectra over a wide range of neutron energies.

To evaluate the effect of this model on the pulse-height spectra, the Cecil et al. code, with the added resolution and threshold calculation above, was modified so that the spectrum was written out as a composite of the response according to the six different reaction channels. For each Monte Carlo event, the light output was calculated as the sum of the light produced by each of the charged particles. The reaction channel which produced the most light for a given event was determined, and an array for that channel was incremented according to the total light output for that event. The sum of the six responses is the total response. The results for the 30×20 cm^2 detector with 10^6 neutrons incident on its flat face at $E_n = 28$, 52.8, and 78.4 MeV are shown in fig. 1; those for $E_n = 88.4$, 138.2, and 198.6 MeV are shown in fig. 2. The six separate reaction channels are identified in the legend.

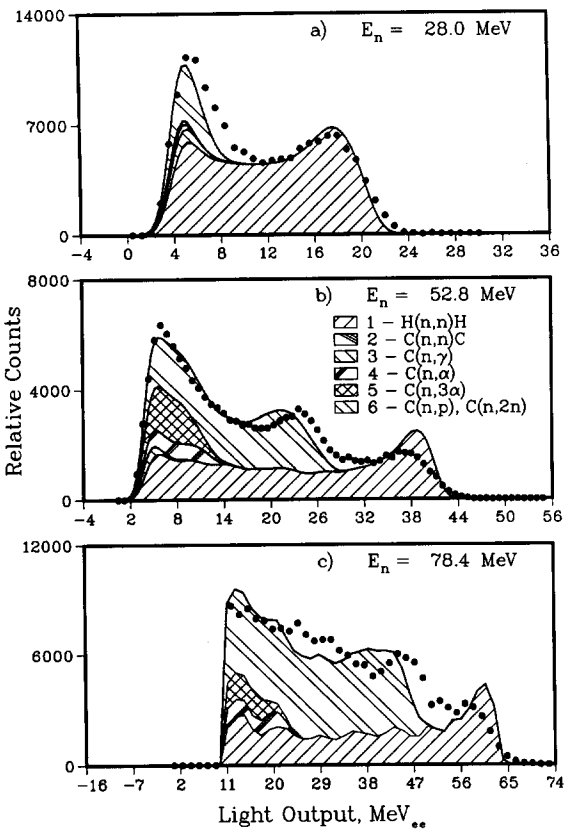

Fig. 1. Calculation of 30×20 cm^2 BC501 scintillator pulse-height spectra, sorted by model reaction channel, for three different incident neutron energies, $28 < E_n < 78.4$ MeV. The calculations are with the unmodified code of Cecil et al., smoothed for resolution effects using eq. (1) with $\sigma_p = 0$. The points are experimental values.

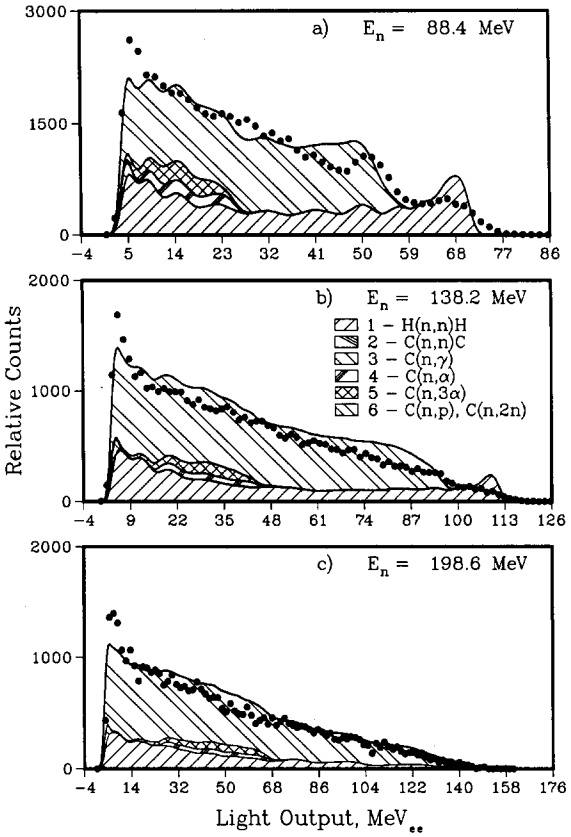

Fig. 2. Calculated pulse-height spectra, sorted by model reaction channel, for $88.4 < E_n < 198.6$ MeV. The calculations are with the unmodified code of Cecil et al., smoothed for resolution effects using eq. (1) with $\sigma_p = 0$.

At the lowest energy, scattering on hydrogen is certainly the most important contributor to the response, followed by carbon breakup, which affects only the lowest light output portion. Even though elastic scattering on carbon is the most frequent reaction, its mean light output is so low that it rarely is the major light producer. As the energy increases, the carbon breakup channel 6 plays a greater role in the shaping of the response. For the data at energies up to 138 MeV, however, the hydrogen scattering channel dominates the highest-energy portion of the curve. At 198 MeV, the maximum proton range is greater than the length of the detector; the high-energy portion of the spectrum is decreased, and the bump present at the high end of the other five curves disappears.

The comparison of pulse-height spectra instead of integral efficiencies enhances the sensitivity to details of the scintillator response. The mismatch between inflections in the data and calculation is quite evident in the $E_n = 88.4$ MeV case, where the edge at 55 MeV$_{ee}$ is not

correctly located by the code. The position of this edge (and the corresponding edges at the other energies) is determined by the kinematics used for the reaction $^{12}C + n \rightarrow {}^{11}B + (n + p)$. The code assumes two-body kinematics; i.e., the fictitious species (n + p) is emitted as a single particle with its mass equal to the neutron-plus-proton mass. The proton then is taken to have a fraction (chosen with a random number generator) of the total (n + p) energy and the neutron the remainder. The edge would move into a position of better agreement with our data if the Q-value for the reaction used the deuteron mass instead of that for (n + p). This suggestion is reinforced by the analysis of Sakai et al., who not only decomposed the calculated response into different channels but also used pulse-shape analysis to identify the recoil particles responsible for different parts of the experimental spectrum. Just above the calculated edge from the carbon breakup channel, there is a peak in the data which the pulse-shape analysis identifies as being due to deuterons from the ^{12}C(n, d) reaction. In our data for $52.8 < E_n < 138$ MeV, the corresponding peak is somewhat lower in light output (possibly from photomultiplier nonlinearity) and is smeared out from poorer resolution. However, it is reasonable to conclude that the use of the (n, d) reaction in the code in place of the (n, np) reaction would give a better representation of both data sets at these energies. This conclusion is also consistent with the experimental findings of McNaughton et al. [9] at $E_n =$ 56 MeV, who found the branching ratio between the two reactions to be roughly equal.

3.2. *Pulse-height spectra by number of scatters*

Another contributor to the shape of the spectra is the influence of multiple scattering of the incident neutron. In order to investigate this effect, the Cecil et al. code (including the threshold and resolution effects, but without changing the reaction model) was modified to produce a spectrum decomposed according to the number of interactions which occur per incident neutron. For brevity, we have chosen not to include figures. At the lowest neutron energies, multiple scattering appears to be very important, but as the energy is increased the spectrum becomes more and more due to single scatters. It is clear that the reason for this decrease is that the total cross section decreases significantly over the energy range. However, we found it difficult to attribute specific features in the pulse-height spectra to specific types of multiple interactions. The relevent quantity is not the number of scatters, but the number which produce an appreciable amount of light. For a multiple scatter of, e.g., two scatters, almost all the light may have been produced by one of the scatters and almost none by the other, especially in the case of the large number of events involving elastic scattering on carbon. The fact that there were two interactions is only incidental.

We found that a more meaningful way to sort the response was according to the number of scatters *on hydrogen*. For example, a neutron which scattered on carbon and then left the detector was counted as zero; if it struck hydrogen only once before causing a ^{12}C(n, p) reaction, it counted as 1 hydrogen scatter, etc. As shown in fig. 3, large amounts of multiple scattering on hydrogen are associated with each of the recoil edges. How this situation occurs is illustrated by an example. The neutron in these cases produces a high-energy recoil proton by n–p scattering at back angles, producing a large amount of light but scattering through a large angle and retaining an energy of maybe only 10 MeV. Below 10 MeV the mean free path is less than the detector dimensions, and the hydrogen cross section is dominant. Because of this the neutron remains in the detector for several more scatters until losing nearly all its energy. The result is a peak located in the spectrum corresponding to all the neutron energy converting to

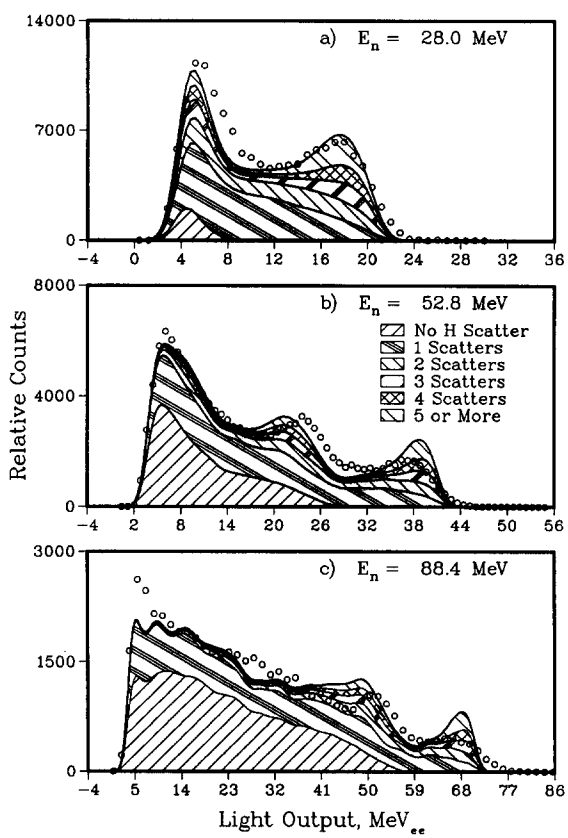

Fig. 3. Calculation of 30×20 cm^2 BC501 scintillator pulse-height spectra, sorted by number of scatters *on hydrogen*, for three different incident neutron energies, $28 < E_n < 88.4$ MeV. The calculations are with the unmodified code of Cecil et al., with resolution effects given by eq. (1) with $\sigma_p = 0$.

recoil proton energy. Obtaining the correct amount of multiple scattering is most important at low incident energies because of low neutron mean free paths and the nonlinearity of the light output curves.

A conspicuous difference between the measured and calculated distributions is in the pronounced rise in the calculated n–p contribution at the highest pulse heights. We checked the differential cross sections and found a coding error which can be traced back at least to Stanton. The angular distribution (calculated in subroutine NPNP) is assumed to be isotropic below 30 MeV. Above 30 MeV the shape is parabolic, using $d\sigma/d\Omega = A + B\cos^2\theta$ with the ratio of the coefficients given by $B/A = E_n/30$. By evaluating these equations for E_n slightly greater than 30 MeV and comparing the results with published values [38], it can be inferred that Stanton probably intended $B/A = E_n/30 - 1$. The result of this coding error is most heavily felt for $30 < E_n < 130$ MeV, where the error increases the peak at the highest light output by about 15%. The error has a significant effect, but not large enough to completely explain the difference in shape.

3.3. Modification for photon loss and attenuation

Nonuniformities in the production and collection of light over the scintillator volume also contribute to the discrepancies between the measured and calculated pulse-height shapes. Our method for calculating this effect is a two-step process. First, the light collection properties of the scintillator/light guide systems under investigation were modeled using the Monte Carlo code GUIDE7 [39]. The result of the calculation is the probability P that a photon emitted at a position (x, y, z) in the scintillator will arrive at the photocathode within the integration time of the electronic circuitry, versus being lost to attenuation, leakage, or absorption. The second step was to modify the subroutine EEQUIV in the Cecil et al. code, which converts energy deposition into light output, to account for this probability map by numerical integration along the particle trajectory of the product of the light output per unit length of track and $P(x, y, z)$.

The input parameters to the transport code are the geometrical surfaces defining the scintillator volume, the light guide system, and the photocathode(s); the photon attenuation length in the medium; and the surface properties. The surfaces of our BC501 scintillator were painted with a diffuse reflector with a high reflectivity of 0.95. Its 45° conical light guide was painted for the third nearest the scintillator and the third nearest the photocathode; the middle third was unpainted and wrapped in black paper. For the photon attenuation length λ a broad range of values is quoted in the literature, with values as low as 38 cm in NE102 plastic scintillator [40]. For NE213, which should be similar to BC501, accepted values range from 150 to 700 cm [41,42]. The value seems to vary with experimental arrangement and may also vary with the age and/or impurity level of the sample. The photocathode was 12.7 cm in diameter; the signal integration assumed that all photons reaching it within the cutoff time of 200 ns would be accepted.

To map out the light-collection probability $P(x, y, z)$, the photon source position was allowed to vary through the volume of the detector, and 3000 photons were emitted at each point. The average collection probability was about 11%, but with a strong positional dependence. Using $\lambda = 120$ cm, P varied from 9.6% at the point in the scintillator volume farthest away from the phototube to 15% at the point nearest. The reason for the strong positional dependence is the 45° angle for the light guide cone, which is apparently too large.

The position variation in light production depends on both the mean interaction distance for incident neutrons and the relationship between range and light output for charged particles in scintillators. For particles with short trajectories the variation in pulse height from event to event will depend simply on the point of origin; for particles with ranges comparable to the detector dimensions the pulse height varies in a more complicated way with trajectory. Integral light output for protons is nearly linear with energy for $E_p > 20$ MeV, but range as a function of energy is not. A 200 MeV proton in BC501 slows at the rate of 5 MeV/cm and produces about 4 MeV_{ee}/cm of light. After it has moved 23 cm, it is 3 cm from its stopping point and is producing about 8 MeV_{ee}/cm of light. More than 50% of the total light is produced in the last 3 cm. The pulse height will be sensitive mostly to where this portion of the track lies in the detector. As a result, at low energies the interaction length for incident neutrons and the range of the charged particles produced are both short, resulting in a strong variation in the light production over the scintillator volume. At higher energies this variation decreases, and the correlation between production and collection in large scintillators becomes less significant.

The calculated change in the pulse-height spectrum with varying photon attenuation length λ in the medium is shown in fig. 4 for $E_n = 52.8$ MeV. The unperturbed calculation is shown with a solid line. Using reasonable values for the attenuation length, photon losses can explain the poor resolution at the largest pulse heights. For the worst case of $\lambda = 60$ cm, a significant shift downward of the proton recoil edge location is seen. Any value for λ between 120 and 400 cm for the BC501 gives adequate agreement with experiment. This variation is because of the significant fraction of the photon losses due to causes other than attenuation; the photons undergo large numbers of surface reflections because of the light guide design.

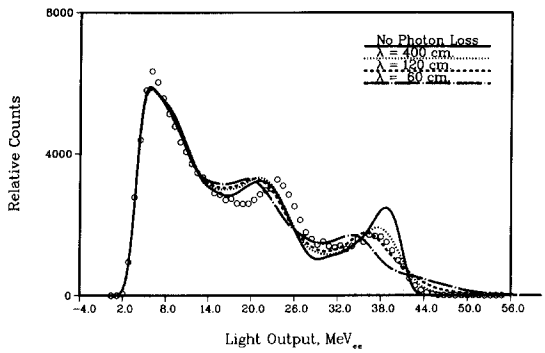

Fig. 4. Calculated variation in the 30×20 cm^2 BC501 scintillator pulse-height spectra with photon attenuation length, for $E_n = 52.8$ MeV. The unmodified calculation is shown with the heavy line.

The primary effect of photon transport is thus an additional contribution to the resolution function. At higher energies or with smaller detectors the light production may be sufficiently uniform that the variation in the light-collection probability P over the volume reduces to a simple σ_p term proportional to pulse height, as in eq. (1). In other cases the correlations between the position dependence of light production and collection can become more important. For instance, if the light produced by protons tends to have a different spatial distribution from that produced by the heavier ions, some relative shifts in pulse-height spectrum features may be seen. Only in the worst cases, however, are the effects of photon transport large enough to cause a sizeable change in the integral efficiency.

4. Extension of the code to medium energies

Over the years, the modifications which led to the code of Cecil et al. (such as adjustments to the cross sections) were usually made to improve the integral efficiency predictions, not the pulse-height spectra. With the changes suggested above, the code should also be able to provide a reasonable reproduction of pulse-height spectra for detectors similar to the one tested here. If the code is to be extended to new domains of applicability, a new approach to its basic reaction model will be required. However, since the integral efficiencies produced with the code below 300 MeV have been verified by experiment many times, any changes to the kinematics should not be allowed to alter the integral efficiency in this region by more than a few percent.

For the carbon breakup channels, no single reaction model can hold over a wide energy range. At energies below ~ 30 MeV, the n–^{12}C interaction is dominated by nuclear structure. The efficiency codes of ref. [15] are an example of the detailed reaction description necessary, and possible, in this region. With increasing energy the number of reaction channels increases rapidly, and there exist neither the comprehensive models nor the detailed measurements needed to continue such an approach. As an example, consider the (n, 3α) reaction, which has been studied more closely since the particular set of reaction channels used in the code was first proposed by Kurz. Up to 35 MeV this reaction has been found to proceed through the 9.6 MeV excited state of ^{12}C followed by sequential alpha decay, in parallel with purely statistical four-body decay and other mechanisms [43]. The four-body phase-space decay mechanism used in the existing code amounts to less than 10% of the cross section. At 57 MeV, the reaction should behave like the charge-symmetric (p, p3α) reaction, which proceeds through sequential α decay; i.e., the proton inelastically scatters, leaving ^{12}C in states of 19 to 27 MeV of excitation energy which then decay by emitting an α-particle [44]. The residual ^{8}Be nucleus promptly splits into two α's.

In contrast to this complexity, at energies of a few hundred MeV all n–^{12}C interactions, including both the ^{12}C(n, 3α) and the ^{12}C(n, p) channels used in the existing code, are expected to become more like free scattering. Collisions of high-energy nucleons with nuclei can then be understood on the basis of models which treat such encounters as a series of nucleon–nucleon interactions [45]. The difference between this "quasi-elastic scattering" and true free scattering is in the binding energy and nuclear momentum distribution. Such a quasi-elastic reaction on an α within the ^{12}C nucleus has been observed [46] at a bombarding proton energy of 150 MeV. The ideal simulation code would combine the low-energy nuclear structure used in the existing code with the straightforward reaction mechanism of high-energy quasi-elastic scattering.

4.1. Changes to reaction kinematics for $70 < E_n < 200$ MeV

The code was modified to use quasi-elastic kinematics for channels 5 and 6 at neutron energies above specific transition energies E_n^{α} and E_n^{p}. Both of these transition energies were adjusted to produce the best description of the measured spectra. Above the energy $E_n^{\alpha} = 70$ MeV, it was found that the (n, 3α) reaction is better described as a quasi-elastic ^{4}He(n, n′)^{4}He reaction. The residual ^{8}Be nucleus (with from 0 to 11 MeV of excitation energy) promptly divides into two alphas which share equally the excitation energy. Above $E_n^{p} =$ 160 MeV, the (n, np) reaction is taken to behave as a quasi-elastic ^{1}H(n, n′)^{1}H reaction. The residual ^{11}B nucleus is taken as having no excitation or kinetic energy. In either reaction the Fermi energy of the nucleon or α within the nucleus is ignored. The reaction cross sections used are exactly those of Cecil et al.

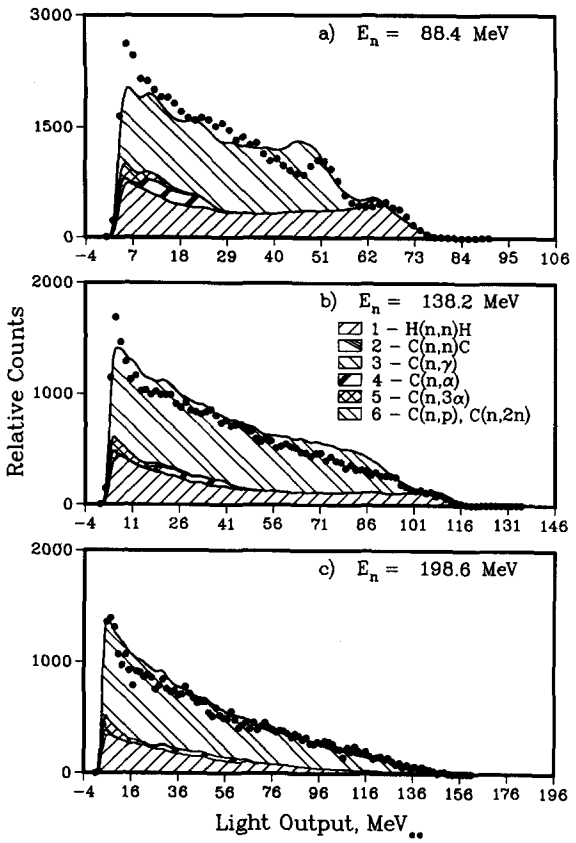

Fig. 5. Calculated pulse-height spectra with the modified code, sorted by model reaction channel, for 88.4 < E_n < 198.6 MeV. The modifications include changes to the kinematics of channels 5 and 6, use of the deuteron mass for the emitted particle in channel 6, corrected angular distributions for n–p free scattering, and the effect of photon losses.

The results for 8×10^5 events are shown in fig. 5 for the Bicron 501 detector at 88, 138 and 200 MeV. Included in the calculations are the three changes previously suggested. The mass of the emitted particle in the ^{12}C(n, np) reaction was changed to that of the deuteron, the shape of the differential cross section for hydrogen elastic scattering was corrected, and the effects of photon losses were calculated using $\lambda = 120$ cm. For $E_n > 70$ MeV, the changes to the kinematics of the ^{12}C(n, 3α) reaction were found to produce a more desired shape to the low pulse-height region. Essentially the entire signal is produced by the α which is directly scattered by the neutron in the quasi-elastic process; the other two α's produce an insignificant signal. The exact shape of the pulse-height spectrum is determined by the angular distribution. In the code, an exponentially forward-peaked distribution was taken. The width of this distribution is significantly broader than the width of the scattering distribution for the ^{4}He(n, n′)^{4}He reaction, which is very forward-peaked [38]. An isotropic center-of-mass distribution also gives a good fit to the data, but is unrealistic. If the ^{4}He(n, n′)^{4}He angular distribution is taken, virtually all the events fall below threshold.

For the 200 MeV calculations, the quasi-elastic process for the ^{12}C(n, np) reaction also applies. Again, the angular distribution determines the shape of the pulse-height distribution. The corresponding free n–p process is very forward- and backward-peaked. In the calculations here, the emitted particles were equally divided between free n–p distribution and an isotropic one.

Although the pulse-height spectra are better described using the modified kinematics, data at higher energies may be needed to determine the best values for E_n^{α} and E_n^{p}. For the relatively high threshold of 3.7 MeV$_{ee}$ used with this detector, the net result of the modifications is an 0.5% drop in efficiency for $E_n > 70$ MeV, due mostly to the changes to the kinematics of channel 5. The other changes in the code have apparently not produced significant change in the integral efficiency, supporting the conclusion that at low thresholds it is largely determined by the total cross sections.

4.2. Code deficiencies for 200 < E_n < 800 MeV

Figs. 1 and 2 showed an increasing trend for the protons to escape the detector with increasing neutron energy. For $E_n = 200$ MeV the proton range has exceeded the 20 cm thickness of the detector. For energies much higher than this, the pulse-height distribution becomes governed largely by particles other than protons.

We have supplemented the IUCF data above with a spectrum obtained recently at the higher energies available at the neutron time-of-flight facility (NTOF) at LAMPF. The NTOF system [3] uses three planes of detector elements, 10 elements stacked vertically per plane. Each element is rectangular in shape, $10.2 \times 10.2 \times 100$ cm^3, with the long axis normal to the flight path. Typically neutrons of between 500 and 800 MeV are detected. A proton in this energy range traversing the 10.2 cm thickness along the incident beam direction can produce at most 30 to 40 MeV$_{ee}$ of light before escaping the detector. On the other hand an α-particle (with its higher stopping power) can produce over 100 MeV$_{ee}$ of light following the same trajectory. Quenching effects, which can diminish the light outputs from high-Z particles at low energies, are less important at these energies.

Fig. 6 shows a pulse-height spectrum obtained recently at NTOF with a monoenergetic beam of 492 MeV neutrons [47]. Shown in the same figure are the calculational results of the unmodified Cecil et al. code. The experimental spectrum has been normalized to have the same integral efficiency as is given by the code.

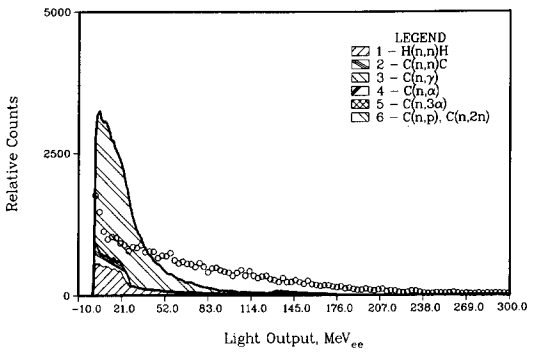

Fig. 6. Comparison of the unmodified code's results with experimental pulse-height spectra obtained at NTOF for E_n = 492 MeV. The experimental values are normalized to the calculation.

Preliminary results from a separate set of NTOF efficiency measurements have shown the code to be good to within 10% over the range $300 < E_n < 730$ MeV for a bias level of 2.4 MeV_{ee} [48]. Consistent with other results in this same energy range [35], the experimental values and calculations for the integral efficiencies appear to be in fairly close agreement.

On the other hand, the calculations clearly lack enough intensity at large pulse heights, a deficiency which must be due to insufficient light output from $Z > 1$ fragments emitted in the carbon breakup channels. One problem with the code may be an insufficient total cross section for α-particle emission, i.e., the true energy dependence of the total cross sections is likely at variance with the code at higher energies. Also there are many possible reaction channels which would emit $Z > 2$ fragments that are not included in the model, e.g., there are no channels which emit lithium ions. This problem is compounded by the light output curve used in the code for all the heavy ions (e.g., ^{9}Be, ^{11}B, or ^{12}C), where it is taken that 0.017 MeV_{ee} of light is created per MeV of particle energy deposited. This ratio has been in the code at least since Stanton. More recent light output values [49] have been found in general to be an order of magnitude greater.

In summary, if the code is to be extended to higher energies, especially for multi-element detectors, a more complete description of the reaction channels for carbon breakup will be needed. Such a description may be possible using one of the existing nuclear physics modeling codes [45]. The light output curves for the heavy ions in this energy range should also be updated at the same time.

5. Conclusions

Many of the features of experimental pulse-height spectra can be explained with the code in terms of the reaction channels or multiple scattering effects; however, its predictions of pulse-height spectra at energies above a few tens of MeV are hampered because of the difficulty in modeling the carbon breakup reaction. Also, due to imperfect photon collection properties in large scintillators, the features of the pulse-height spectra tend to blur out. Modifying the reaction kinematics at neutron energies over 70 MeV so as to make a transition to quasi-elastic reaction kinematics tends to give improved predictions of pulse-height spectra up to 200 MeV. Extending the validity of the code's pulse-height spectra predictions up to 800 MeV in energy will require substantial reworking of the model reaction channels and the code's light output curves.

Acknowledgement

The original copy of the Monte Carlo code of Cecil et al. was provided by B.D. Anderson of Kent State University.

References

[1] R.A. Cecil, B.D. Anderson and R. Madey, Nucl. Instr. and Meth. 161 (1979) 439.
[2] T.N. Taddeucci et al., Nucl. Instr. and Meth. A241 (1985) 448.
[3] J.B. McClelland, 3rd Int. Conf. on Spin Observables of Nuclear Probes, Telluride, CO, USA (1988).
[4] J.R.M. Annand, G.I. Crawford and R.O. Owens, Nucl. Instr. and Meth. A262 (1987) 329.
[5] J.A. Strong et al., Nucl. Instr. and Meth. 156 (1978) 411.
[6] S. Cierjacks et al., Nucl. Instr. and Meth. A238 (1985) 354.
[7] R.C. Byrd and W.C. Sailor, Nucl. Instr. and Meth. A274 (1989) 494.
[8] N.R. Stanton, COO-1545-92, Ohio State University (February, 1971).
[9] M.W. McNaughton, N.S.P. King, F.P. Brady and J.L. Ullmann, Nucl. Instr. and Meth. 129 (1975) 241. Note: An important feature introduced by McNaughton et al. is the division of the ^{12}C(n, p) reaction (channel 6) into three reactions, the most important of which is the ^{12}C(n, np) reaction. They state that the angular distribution for proton emission should be taken as forward-peaked with probability proportional to $\cos\theta_p$ in the *laboratory* frame. However, in the code of Cecil et al. it is the *center-of-mass* angle that has this distribution. Our code follows the prescription of Cecil et al.
[10] R.J. Kurz, UCRL-11339, Berkeley, CA, USA (1964).
[11] R. De Leo, G. D'Erasmo, A. Pantaleo and G. Russo, Nucl. Instr. and Meth. 119 (1974) 559.
[12] M. Anghinolfi, G. Ricco, P. Corvisiero and F. Masulli, Nucl. Instr. and Meth. 165 (1979) 217.
[13] R.E. Textor and V.V. Verbinski, ORNL-4160, Oak Ridge National Laboratory (1968).

[14] Y. Umamino, K. Shin, M. Fujii and T. Nakamura, Nucl. Instr. and Meth. 204 (1982) 179.
[15] G. Dietze and H. Klein, PTB-Bericht ND-22 (October, 1982).
[16] A. Del Guerra, Nucl. Instr. and Meth. 135 (1976) 337.
[17] D.A. Kellogg, Phys. Rev. 90 (1953) 224.
[18] R. Madey et al., Nucl. Instr. and Meth. 151 (1978) 445.
[19] C.E. Wiegand, UCRL-9986, Berkeley, CA, USA (1961).
[20] R.M. Edelstein et al., Nucl. Instr. and Meth. 100 (1972) 355.
[21] D.G. Crabb, J.G. McEwen, E.G. Auld and A. Langsford, Nucl. Instr. and Meth. 48 (1967) 87.
[22] F.P. Brady, J.A. Jungermann, J.C. Young, J.L. Romero and P.J. Symonds, Nucl. Instr. and Meth. 58 (1968) 57.
[23] J.B. Hunt et al., Nucl. Instr. and Meth. 85 (1970) 269.
[24] J.C. Young, J.L. Romero, F.P. Brady and J.R. Morales, Nucl. Instr. and Meth. 68 (1969) 333.
[25] G. Betti et al., Nucl. Instr. and Meth. 135 (1976) 319.
[26] A.S.L. Parsons et al., Nucl. Instr. and Meth. 79 (1970) 43.
[27] M. Drosg, Nucl. Instr. and Meth. 105 (1972) 573.
[28] R.A.J. Riddle, G.H. Harrison, P.G. Roos and M.J. Saltmarsh, Nucl. Instr. and Meth. 121 (1974) 445.
[29] S.T. Thornton and J.R. Smith, Nucl. Instr. and Meth. 96 (1971) 25.
[30] B.D. Anderson, J.N. Knudson, R. Madey and C.C. Foster, Nucl. Instr. and Meth. 169 (1980) 153.
[31] R. Madey et al., Nucl. Instr. and Meth. 214 (1983) 401.
[32] J.W. Watson et al., Nucl. Instr. and Meth. 215 (1983) 413.
[33] P.T. Debevec, G.L. Moake and P.A. Quin, Nucl. Instr. and Meth. 166 (1979) 467.
[34] S. Cierjacks et al., Nucl. Instr. and Meth. 192 (1982) 407.
[35] S.D. Howe, P.W. Lisowski, G.J. Russell, N.S.P. King and H.J. Donnert, Nucl. Instr. and Meth. 227 (1984) 565.
[36] H. Sakai, N. Matsuoka, T. Saito and A. Sakaguchi, Nucl. Instr. and Meth. A247 (1986) 515.
[37] H. Scholermann and H. Klein, Nucl. Instr. and Meth. 169 (1980) 25.
[38] D.I. Garber, L.G. Stromberg, M.D. Goldberg, D.E. Cullen and V.M. May, BNL-400, 3rd ed., vol. 1, Brookhaven (January, 1970).
[39] T. Massam, CERN 76-21 (1976).
[40] G. Keil, Nucl. Instr. and Meth. 87 (1970) 111.
[41] P. Kuijper, C.J. Tiesinga and C.C. Jonker, Nucl. Instr. and Meth. 42 (1966) 56.
[42] V.V. Filchenkov, A.D. Konin and V.G. Zinov, Nucl. Instr. and Meth. A245 (1986) 490.
[43] B. Antolkovic, I. Slaus, D. Plenkovic, P. Macq and J.P. Meulders, Nucl. Phys. A394 (1983) 87.
[44] M. Epstein et al., Phys. Rev. 178 (1969) 1698.
[45] T.S. Subramanian et al., Phys. Rev. C28 (1983) 521.
[46] A.N. James and H.G. Pugh, Nucl. Phys. 42 (1963) 441.
[47] T.N. Taddeucci, MP Division, Los Alamos National Laboratory, private communication.
[48] L.J. Rybarcyk et al., Bull. Am. Phys. Soc. 33 (1988) 1578.
[49] P.D. Becchetti, C.E. Thorn and M.J. Levine, Nucl. Instr. and Meth. 138 (1976) 93.